Journal of Advanced Research in Numerical Heat Transfer

Journal homepage:
https://semarakilmu.com.my/journals/index.php/arnht/index
ISSN: 2735-0142

Thermal and Flow Characteristics of Alumina Nanofluids in Microfluidic Systems: A Low-Concentration Study

Lingenthiran Samylingam[1], Navid Aslfattahi [2,] Kumaran Kadirgama[3,4,5*], Devarajan Ramasamy[3], Chee Kuang Kok[1], Norazlianie Sazali[5,6], Wan Sharuzi Wan Harun[3,7], Nor Atiqah Zolpakar[3,5], Mohd Fairusham Ghazali[5]

[1] Centre for Advanced Mechanical and Green Technology, Faculty of Engineering and Technology, Multimedia University, Jalan Ayer Keroh Lama, Bukit Beruang, 75450 Melaka, Malaysia
[2] Institute of Fluid Dynamics and Thermodynamics, Faculty of Mechanical Engineering, Czech Technical University in Prague, Technická 4, 166 07 Prague, Czech Republic
[3] Faculty of Mechanical & Automotive Engineering Technology, Universiti Malaysia Pahang, 26600 Pekan, Pahang, Malaysia
[4] College of Engineering, Almaaqal University, Basra, 61003, Iraq
[5] Centre for Research in Advanced Fluid and Processes, University Malaysia Pahang Al-Sultan Abdullah, 26600 Pekan, Pahang, Malaysia
[6] Faculty of Manufacturing and Mechatronic Engineering Technology, University Malaysia Pahang, 26600 Pekan, Pahang, Malaysia
[7] Centre for Automotive Engineering, Universiti Malaysia Pahang Al-Sultan Abdullah, Malaysia

ARTICLE INFO

Article history:
Received 24 September 2024
Received in revised form 25 October 2024
Accepted 22 November 2024
Available online 15 December 2024

Keywords:
Microfluidic technologies; Heat transfer; Thermal management; Alumina (Al_2O_3)

ABSTRACT

Microfluidic technologies and nanofluids represent a synergistic combination with significant potential for enhancing heat transfer and thermal management applications. This study investigates the thermal and flow characteristics of a 0.001 wt.% alumina (Al_2O_3)-water nanofluid within a custom-designed serpentine microfluidic channel. The nanofluid was prepared and characterized for its thermal conductivity, viscosity, specific heat, and density. Experimental microfluidic studies, supplemented by numerical simulations, were conducted to evaluate the fluid's behavior under controlled conditions. Results indicated a slight increase in thermal conductivity for the Al_2O_3 nanofluid compared to pure water, with increments ranging from 0.16% at 20°C to 0.30% at 80°C, attributed to enhanced Brownian motion of the nanoparticles. Viscosity measurements revealed marginal increases, suggesting minimal impact on fluid flow dynamics. The microfluidic experiments demonstrated a consistent pressure gradient and laminar flow regime, essential for precise control and efficient thermal management. Temperature contours showed effective heat dissipation, with a steady thermal gradient from the inlet to the outlet. The study concludes that low-concentration Al_2O_3 nanofluids can enhance thermal performance in microfluidic systems without significantly affecting flow characteristics, making them suitable for applications requiring efficient heat dissipation, such as electronic cooling and chemical reactions. These findings provide a foundation for future research into higher nanoparticle concentrations and different base fluids, aimed at optimizing the thermal and flow properties of nanofluids in microfluidic environments. The integration of nanofluids with microfluidic technologies holds promise for advancing the performance and reliability of next-generation thermal management systems.

* *Corresponding author.*
E-mail address: kumaran@umpsa.edu.my (Kumaran Kadirgama)

https://doi.org/10.37934/arnht.28.1.131144

1. Introduction

In recent years, microfluidic technologies have revolutionized various fields, including biomedical engineering, chemical synthesis, and energy systems, by enabling precise manipulation of fluids at the microscale [1-3]. This advancement is particularly significant in the development of nanofluids, which are engineered colloidal suspensions of nanoparticles in a base fluid [4]. Nanofluids exhibit enhanced thermal properties, such as thermal conductivity and heat capacity, which make them promising candidates for applications in heat transfer and cooling systems [5,6]. The integration of nanofluids with microfluidic systems presents a unique opportunity to exploit the synergistic effects of both technologies. Microfluidic platforms offer precise control over fluid flow, mixing, and heat transfer, while nanofluids provide superior thermal properties that can significantly enhance the performance of these systems [7]. This combination is particularly relevant for applications requiring efficient heat dissipation, such as electronic cooling, and energy storage systems [8,9]. The focus of this study is to investigate the thermal and flow characteristics of low-concentration alumina (Al_2O_3) nanofluid in a microfluidic environment. The specific objectives are to prepare a stable 0.001 wt.% Al_2O_3-water nanofluid, characterize its thermal and physical properties and analyze its performance in a custom-designed microfluidic setup. By comparing the experimental results with baseline measurements using pure water, this study aims to provide insights into the potential benefits and limitations of using nanofluids in microfluidic applications. To achieve these objectives, a comprehensive methodology was employed, encompassing the preparation and characterization of the nanofluid, the design and execution of microfluidic experiments, and the application of numerical simulations to validate the experimental findings. This multi-faceted approach ensures a thorough understanding of the interplay between nanofluid properties and microfluidic behavior, laying the groundwork for future developments in this field. The following sections detail the preparation and characterization of the Al_2O_3 nanofluid, the experimental setup for microfluidic studies, the boundary conditions and simulation parameters, and the results obtained from both experimental and numerical analyses. Through this systematic investigation, the study aims to advance the knowledge of nanofluid dynamics in microfluidic systems, thereby contributing to the optimization of thermal management solutions in various technological applications.

2. Methodology

2.1 Nanofluid Preparation

High-purity alumina oxide nanoparticles with an average size ranging from 20- 50 nanometers were purchased from US Research Nanomaterials, Inc. (Houston, TX, USA). 100 ml of distilled water was prepared. Then the Al_2O_3 nanoparticles were measured and added to the distilled water while stirring it with a hotplate stirrer for an hour at 300 rpm. Later the mixture was sonicated using an ultrasonicator for an hour at 70% power and 7/3 s on/off to form a 0.001 wt.% of Al_2O_3 -water nanofluid.

2.2 Characterization

The morphology of Al_2O_3 nanoparticles was inspected with a scanning electron microscope (SEM). The operating voltage and current were 15 kV and 10 mA, respectively. The thermal conductivity of the prepared 0.001 wt% Al_2O_3 nanofluid was studied using KS-3 sensor temperature ranging from 20 – 80 ℃. The viscosity was measured with a rheometer (MCR 92, Anton Paar, Austria) with temperatures ranging from 20 – 80 ℃. The specific heat was studied by using Perkin Elmer/ DSC 8000

with temperatures ranging from 20 – 80 ℃. Density was measured by using a Density meter/Anton Paar with temperature ranging from 20 – 80 ℃.

2.3 Microfluidic Experiment

The setup consists of a syringe pump (model: SN-50F6), a differential pressure transmitter (model: STK336), a custom-made microchannel, connections, and a collection beaker. The assembly begins with a syringe pump with two syringes connected with a T-connection, and a micro-tube, respectively. The outlet of this microtube is directed to another T-joint. One of the outlets of the T-joint is directed to the differential pressure transmitter, which measures the channel inlet pressure, whereas the other outlet is directly connected to a microchannel through a micro-tube. The outlet of this microchannel is connected to another T-joint, one of the outlets of the T-joint is connected to the differential pressure transmitter, which measures the outlet pressure. ELVEFLOW FLOW- A 5 sensor was used to measure the flow rate. The flow rate for the microfluidic was kept constant at 300 µl/min. The image for the 0.001% Al_2O_3 nanofluid was captured using a DOLOMITE NIKON/SMZ745T high-speed camera microscope. Figure 1 shows the schematic diagram of the experimental setup for the microfluidic study. The pressure for the microfluidic was monitored by using an ELVEFLOW/ELVEFLOW SMART INTERFACE.

The choice of the serpentine (snake-like) microchannel design in this study was deliberate, as it offers several significant benefits for enhancing both heat transfer and fluid flow in microfluidic systems. One of the primary advantages of the serpentine structure is its ability to increase the surface area available for heat exchange between the nanofluid and the channel walls. The extended path length of the serpentine design allows the nanofluid more time to dissipate heat, making it particularly suitable for applications that demand efficient thermal management. This increased interaction between the fluid and the channel walls contributes to superior thermal performance compared to simpler designs. Furthermore, the serpentine design promotes laminar flow stability, which is critical in microfluidic systems that operate at low Reynolds numbers. The design ensures that the flow remains steady and predictable, avoiding turbulence that could disrupt fluid movement and reduce the effectiveness of thermal management. The gradual pressure drops and consistent flow trajectory throughout the serpentine channel help maintain this laminar flow, preventing sudden flow disruptions that could lead to clogging or particle accumulation. This is particularly important in systems using nanofluids, as maintaining smooth flow ensures that the nanoparticles remain suspended and do not settle or agglomerate, which could otherwise obstruct the channel.

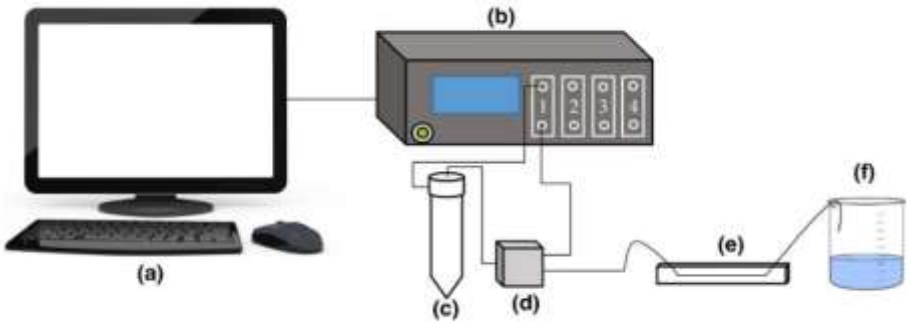

Fig. 1. Schematic diagram of the experimental setup consists of (a) computer, (b) pressure and vacuum controller, (c) reservoir containing nanofluid, (d) flow sensor, (e) microfluidic channel, and (f) beaker as storage tank

2.4 Boundary Condition

Figure 2(a) and 2(b) shows the setup used for the simulation. The Inlet Total pressure is 20000 Pa and the environment outlet was set similar to the experimental setup. The flow is targeted from the inlet to the outlet via the design. The total meshing was 807,083 fluid cells with quadrilateral mesh elements.

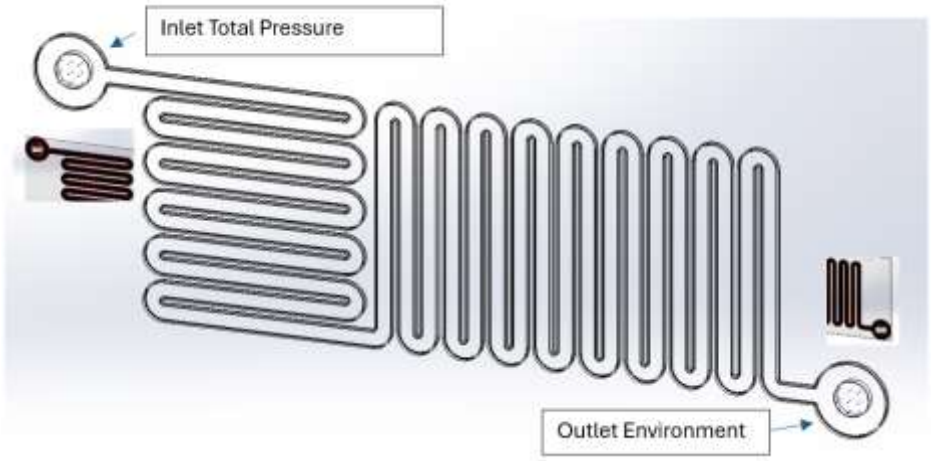

(a)

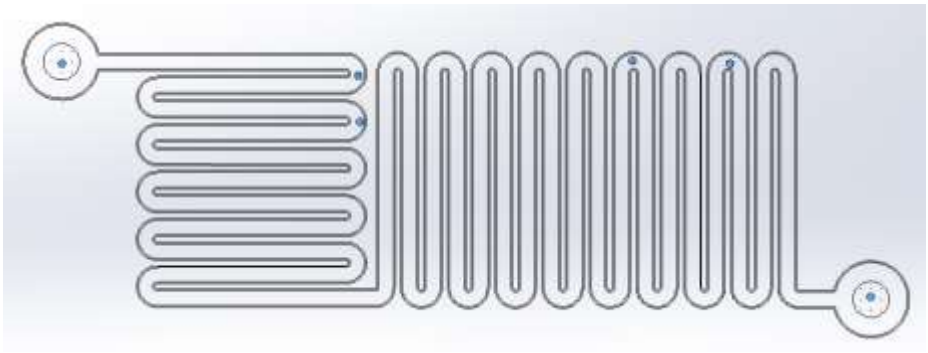

(b)

Fig. 2. (a) setup used for simulation (b) The points are taken for temperature comparison

The standard laminar fluid flow equations including continuity, momentum conservation, and energy equations inside the microchannel cold plates have been considered as follows [10]:

$$\nabla \cdot (\rho \vec{v}) = 0\,, \tag{1}$$

$$\rho \frac{\partial \vec{v}}{\partial t} + \nabla \cdot (\rho \vec{v}\vec{v}) = -\nabla P + \mu \nabla^2 \vec{v}\,, \tag{2}$$

$$\rho C_p \frac{\partial T}{\partial t} + \nabla \cdot \left(\rho C_p \vec{v} T\right) = \nabla \cdot (k \nabla T)\,, \tag{3}$$

where ρ is density, $\vec{v}$ is velocity vector, t is time, P is pressure, μ is dynamic viscosity, C_p is specific heat capacity, T is temperature, and k is thermal conductivity. All quantities are evaluated in the liquid phase.

A few points from the setup were taken for temperature comparisons. Figure 2(b) shows the temperature taken at this point in the design. The blue dots show the points. The points are taken on the bends, inlet, and outlet.

The parameters used for the simulations, including mesh details, boundary conditions, and thermophysical properties of the nanofluid, are summarized in Table 1 below. The properties of the Al_2O_3 nanofluid (density, specific heat, thermal conductivity, and viscosity) were obtained from experimental measurements to ensure consistency between the simulations and experiments.

Table 1
The simulation parameters

Parameters	Value/Method	Description
Solver	ANSYS Fluent (Laminar Model)	CFD software is used for simulation, solving the laminar flow equations
Mesh Type	Quadrilateral (2D)	Structured quadrilateral mesh was used to discretize the microchannel geometry
Total Mesh Cells	807,083 cells	Number of cells used for the simulation
Inlet Boundary Condition	Inlet Pressure = 20000 Pa	Total pressure applied at the inlet of the microchannel
Outlet Boundary Condition	Outlet Pressure = 0 Pa (atmospheric)	Set at ambient pressure to mimic experimental conditions
Fluid Type	0.001 wt.% Al_2O_3-water nanofluid	The same nanofluid used in the experiments
Thermal Conductivity	0.600–0.672 W/mK (measured)	Measured thermal conductivity of the nanofluid at various temperatures (20–80°C)
Viscosity	1.005–0.355 mPa.s (measured)	Measured viscosity of the nanofluid at various temperatures (20–80°C)
Density	998.24–971.83 kg/m³ (measured)	The measured density of the nanofluid at various temperatures (20–80°C)
Specific Heat	4.180–4.168 kJ/kg°C (measured)	Measured specific heat of the nanofluid at various temperatures (20–80°C)
Flow Rate	300 µl/min	The same flow rate used in the experimental setup
Simulation Time Step	0.001 s	The time step used for transient simulations
Heat Transfer Coefficient	Computed based on nanofluid properties	Derived from fluid properties and used in the energy equation
Reynolds Number	1.35 (calculated)	Calculated based on the flow rate, viscosity, and microchannel geometry

3. Results

3.1 Characterization

Figure 3 shows the SEM and EDX analysis of Al_2O_3 nanoparticles. Based on the EDX analytical results in the paper, the sample consists of carbon (C), oxygen (O), and aluminum (Al). The mass percentages for carbon, oxygen, and aluminum are roughly 6.55%, 48.77%, and 44.68% respectively, totaling 100%. The sample consists of 10.39% carbon, 58.07% oxygen, and 31.54% aluminum when examining the atomic percentages. The carbon detected in the sample originated from the carbon duct tape used during the sample preparation procedure.

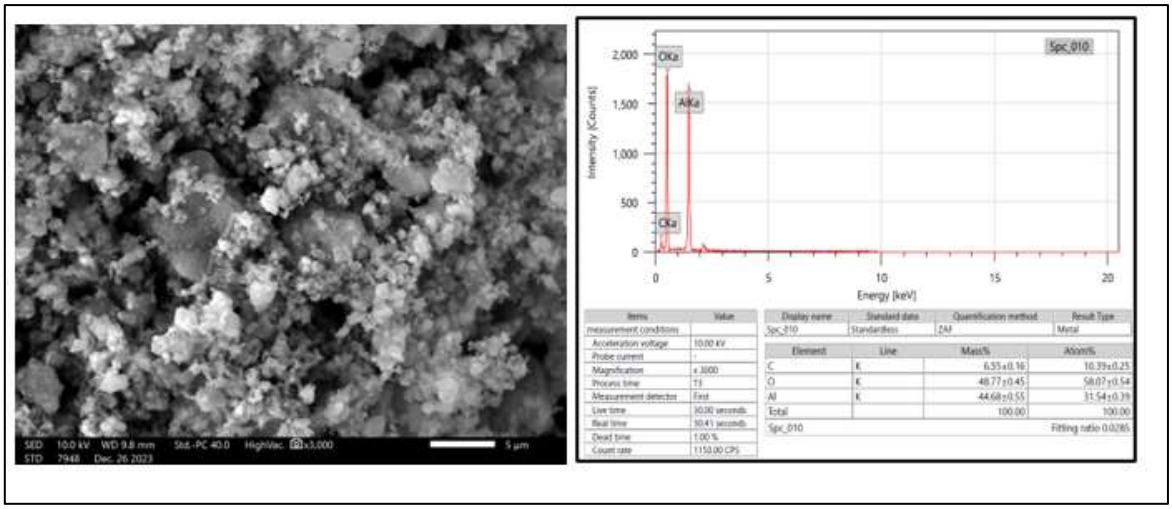

Fig. 3. SEM and EDX analysis of Al_2O_3 nanoparticles.

Table 2 shows the results obtained from thermal conductivity, viscosity, specific heat, and density measurements for water and 0.001 wt% Al_2O_3 -water nanofluid. At 20 ℃ water shows 0.598 W/mk. Then slowly increase to 0.631, 0.654, and 0.670 W/mK at 40 ℃, 60 ℃, and 80 ℃ respectively. Thermal conductivity for 0.001% Al_2O_3 at 20 ℃ is 0.600 W/mK, at 40 ℃ is 0.633 W/mK, at 60 ℃ is 0.656 W/mK and at 80 ℃ is 0.672 W/mK. The thermal conductivity of the 0.001% Al_2O_3 nanofluid is only slightly higher than the base fluid (water) for all the temperatures ranging from 20 – 80 ℃. The percentage increment is from 0.16% at 20 ℃ to 0.30 % at 80 ℃. The reason for the slight increment is due to the increased Brownian motion in nanofluids because of the nanoparticles [11].

Viscosity for water at 20 ℃ is 1.002 mPa.s, then slowly decrease at 40 ℃ to 0.653 mPa.s. Then when the temperature increases to 60 ℃ and 80 ℃ the viscosity of water is 0.467 mPa.s and 0.355 mPa.s respectively. Viscosity for 0.001% Al_2O_3 at 20 ℃ is 1.005 mPa.s, at 40 ℃ is 0.655 mPa.s, at 60 ℃ is 0.468 mPa.s and at 80 ℃ is 0.355 mPa.s. The viscosity of the 0.001% Al_2O_3 nanofluid is only slightly higher than the base fluid (water) for all the temperatures ranging from 20 – 60 ℃. At 80 ℃ the viscosity reading for both water and 0.001% Al_2O_3 is similar which is 0.355 mPa.s. Chandrasekar *et al.,* [9] studied the viscosity of the nanofluids for Al_2O_3 nanoparticles in water. They disclosed that the viscosity rises linearly by upgrading particle concentration up to the concentration of 2%. The main cause of the rise in viscosity in nanofluids is the interaction between the nanoparticles and the molecules of the base fluid [12,13]. Nanoparticles, enhance the structural complexity of the fluid. The complexity arises from the increased surface interactions between the nanoparticles and the fluid molecules, as well as among the nanoparticles themselves. These interactions frequently involve van der Waals forces, electrostatic forces, and steric effects, which collectively form a network within the fluid [12]. These networks can impede the unrestricted movement of the fluid, thus augmenting its viscosity.

Additionally, similar trends of small but consistent increases in thermal conductivity and viscosity have been reported in the literature for low-concentration nanofluids. Studies such as Koo and Kleinstreuer [14], Puliti [15], and Soares *et al.,* [16] have shown that nanoparticle concentrations as low as 0.001 wt.% can still result in measurable changes in fluid properties due to enhanced Brownian motion and particle-fluid interactions. These findings are in line with our results, where even small concentrations of alumina nanoparticles contribute to slight but detectable improvements in thermal performance and fluid dynamics.

Table 2
The properties of Al_2O_3

Temperature (℃)		20	40	60	80
Thermal Conductivity (W/mK)	Water	0.599	0.631	0.654	0.670
	0.001% Al_2O_3	0.600	0.633	0.656	0.672
Viscosity (mPa.s)	Water	1.002	0.653	0.467	0.355
	0.001% Al_2O_3	1.005	0.655	0.468	0.355
Specific heat (kJ/kg℃)	Water	4.181	4.178	4.175	4.172
	0.001% Al_2O_3	4.180	4.176	4.172	4.168
Density (kg/m^3)	Water	998.20	992.20	983.20	971.80
	0.001% Al_2O_3	998.24	992.24	983.24	971.83

Specific heat for water at 20 ℃ is 4.181 kJ/kg℃, then slowly decrease at 40 ℃ to 4.178 kJ/kg℃. Then when the temperature increases to 60 ℃ and 80 ℃, the specific heat of water is 4.175 kJ/kg℃, and 4.172 kJ/kg℃ respectively. Specific heat for 0.001% Al_2O_3 at 20 ℃ is 4.180 kJ/kg℃, at 40 ℃ is 4.176 kJ/kg℃, at 60 ℃ is 4.172 kJ/kg℃ and at 80 ℃ is 4.168 kJ/kg℃. The specific heat of the 0.001% Al_2O_3 nanofluid is reducing compared to the base fluid (water) for all the temperatures ranging from 20 – 80 ℃. This phenomenon is due to the addition of nanoparticles to the base fluid [17].

The density of water at 20 ℃ is 998.20 kg/m^3, at 40 ℃ is 992.20 kg/m^3 at 60 ℃ is 983.20 kg/m^3, and at 80 ℃ is 971.80 kg/m^3. The density of 0.001% Al_2O_3 at 20 ℃ is 998.24 kg/m^3, at 40 ℃ is 998.24 kg/m^3, at 60 ℃ is 998.24 kg/m^3 and at 80 ℃ is 971.83 kg/m^3. The density of the 0.001% Al_2O_3 nanofluid is only slightly higher than the base fluid (water) for all the temperatures ranging from 20 – 80 ℃. The minimal rise in the density of a 0.001 wt% Al_2O_3 -water nanofluid at different temperatures is mainly due to the extremely low amount of the dense nanoparticles and their even distribution within the water [18]. This scenario demonstrates that even materials with great density can have little effect on a solution when present in very low quantities.

3.2 Pressure Plots

Figure 4 illustrates the pressure distribution of a microfluidic system containing a 0.001 wt.% Al_2O_3-water nanofluid. The microchannel is designed in a serpentine pattern to maximize the interaction between the fluid and the channel walls, which is crucial for applications that rely on efficient heat transfer and fluid mixing. The figure shows a distinct pressure gradient from the inlet (red) to the outlet (blue). The highest pressure is observed at the inlet, with a gradual decrease along the length of the channel. This pressure drop is indicative of laminar flow, which is typical in microfluidic systems due to the small dimensions and low Reynolds numbers involved [19]. The red region near the inlet indicates the highest pressure, approximately 13124.43 Pa. This high-pressure zone is critical as it drives the fluid through the microchannel. The pressure drop across the channel is essential for maintaining a steady flow rate, which, in this case, is kept constant at 300 µl/min. The high-pressure region also suggests that the fluid encounters significant resistance as it enters the narrow channels, which is a common characteristic in microfluidic systems due to the small cross-sectional area [20]. As the fluid progresses through the serpentine channel, the pressure gradually decreases, transitioning from red to green. This mid-pressure region indicates a smooth flow transition, where the fluid loses pressure due to frictional forces between the fluid and the channel walls [21]. The serpentine design helps in maintaining a controlled pressure drop, ensuring that the fluid has adequate time for heat transfer and mixing. The blue region near the outlet represents the lowest pressure, around 10449.90 Pa. This low-pressure zone is crucial for drawing the fluid through the entire length of the microchannel. The gradual pressure decrease ensures that the fluid maintains

a laminar flow, which is necessary for precise control in microfluidic applications [22]. The consistent pressure drop also indicates that there are no significant blockages or disruptions within the channel, which is vital for the reliability and efficiency of the system. The pressure contours depicted in the figure are vital for understanding the behavior of nanofluids in microfluidic systems. The steady pressure gradient ensures a uniform flow rate, which is essential for applications involving heat transfer, chemical reactions, and biological assays [1]. The laminar flow regime, indicated by the smooth pressure transition, is beneficial for minimizing fluid disturbances and achieving consistent results.

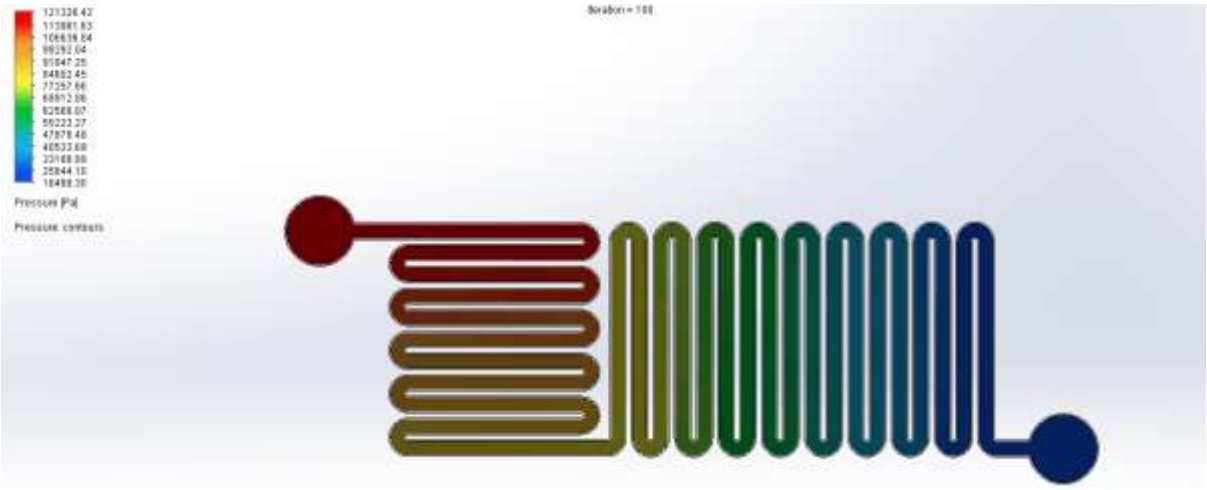

Fig. 4. Pressure distribution of a microfluidic system containing a 0.001 wt.% Al_2O_3-water nanofluid

3.3 Velocity Plots

Figure 5 shows the fluid dynamic within the microfluidic channel of 0.001 wt.% Al_2O_3-water nanofluid. The red regions indicate the highest fluid velocities, reaching up to 1.50e-04 m/s. These high-velocity zones are predominantly observed at the channel's inlet and outlet. The elevated velocities at these points are due to the initial momentum imparted to the fluid by the syringe pump at the inlet and the pressure-driven flow toward the outlet [23]. These high velocities are essential for ensuring that the fluid enters and exits the microchannel efficiently, maintaining a consistent flow rate throughout the system [24]. As the fluid traverses the serpentine path, the velocity decreases, transitioning from red to green. This reduction in velocity is indicative of the frictional forces encountered by the fluid as it flows through the narrow channels [25]. The serpentine design increases the path length, which helps in dissipating the fluid's kinetic energy gradually, ensuring a more uniform flow distribution. The mid-velocity regions signify areas where the fluid maintains a steady flow, which is crucial for effective heat transfer and mixing processes within the microchannel [26]. The blue regions near the inlet and outlet, as well as at certain bends within the channel, indicate the lowest velocities, around 1.10e-04 m/s. These low-velocity zones are typically areas of recirculation or stagnation, where the fluid experiences a reduction in speed due to changes in direction or geometric constraints. The presence of low-velocity regions at the bends of the serpentine channel is expected, as the fluid must navigate sharp turns, which temporarily slows down its movement. These areas are critical for enhancing mixing and ensuring that the entire fluid volume is exposed to the channel walls, facilitating efficient thermal exchange. The velocity contours shown in Figure 5 provide valuable insights into the fluid dynamics within the microfluidic channel. The consistent velocity gradient from inlet to outlet and the smooth transition between high and low-velocity regions indicate a well-designed microfluidic system capable of maintaining laminar flow

[27]. This is essential for applications requiring precise control over fluid movement, such as chemical reactions, biological assays, and heat transfer processes. Moreover, the observed velocity distribution suggests that the serpentine channel effectively manages the fluid flow, ensuring that the nanofluid experiences adequate mixing and heat transfer. The balance between high and low-velocity regions helps in optimizing the performance of the microfluidic device, making it suitable for various technological applications.

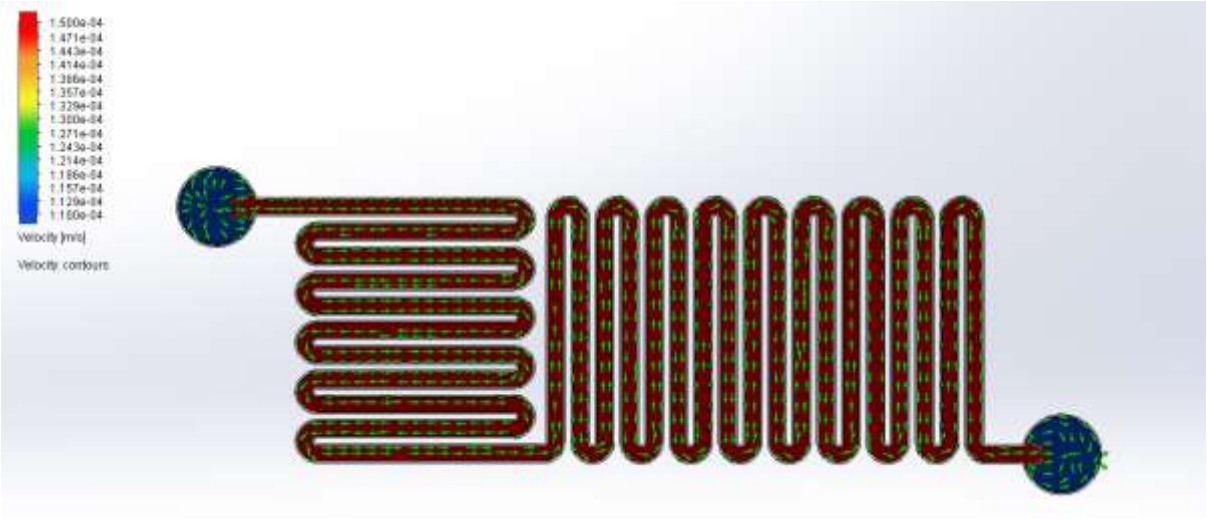

Fig. 5. Fluid dynamic within the microfluidic channel

3.4 Temperature Plots

Figure 6 illustrates the temperature contour within the microfluidic channel 0.001 wt.% Al_2O_3-water nanofluid. The temperature contours highlight the variations in fluid temperature across different sections of the microchannel, offering insights into the thermal behavior of the nanofluid as it flows through the system. The red region near the inlet indicates the highest temperature, approximately 311.24 K. This high-temperature zone is critical as it represents the initial thermal condition of the nanofluid as it enters the microchannel [28]. The elevated temperature at the inlet ensures that the fluid has sufficient thermal energy to transfer as it moves through the channel, which is essential for applications involving heat dissipation or thermal management. As the fluid progresses through the serpentine channel, the temperature gradually decreases, transitioning from red to blue. This temperature gradient indicates effective heat dissipation along the length of the channel [29]. The serpentine design, with its extended path length, enhances the surface area for heat exchange, allowing the fluid to lose thermal energy efficiently to the channel walls and the surrounding environment [30]. This gradual temperature reduction is vital for maintaining a steady thermal condition within the microfluidic system, ensuring that the fluid exits at a lower temperature, around 291.10 K, as indicated by the green and blue regions near the outlet. The yellow and green regions in the middle sections of the channel indicate mid-range temperatures, typically between 297 K and 303 K. These regions signify areas where the fluid maintains a relatively stable temperature, balancing between heat loss and the initial thermal energy. The mid-temperature zones are crucial for applications requiring uniform thermal conditions, as they ensure that the fluid does not experience abrupt temperature changes, which could affect the overall performance of the microfluidic system [31]. The temperature contours depicted in Figure 6 are essential for understanding the thermal management capabilities of the microfluidic system. The consistent temperature gradient from the inlet to the outlet indicates effective thermal control, which is crucial

for applications such as electronic cooling, chemical reactions, and biological assays that require precise temperature regulation [32-36]. Moreover, the temperature distribution suggests that the addition of Al_2O_3 nanoparticles enhances the thermal conductivity of the base fluid, facilitating efficient heat transfer [37]. The presence of nanoparticles likely improves the fluid's ability to absorb and dissipate thermal energy, ensuring that the temperature drop is smooth and consistent throughout the channel.

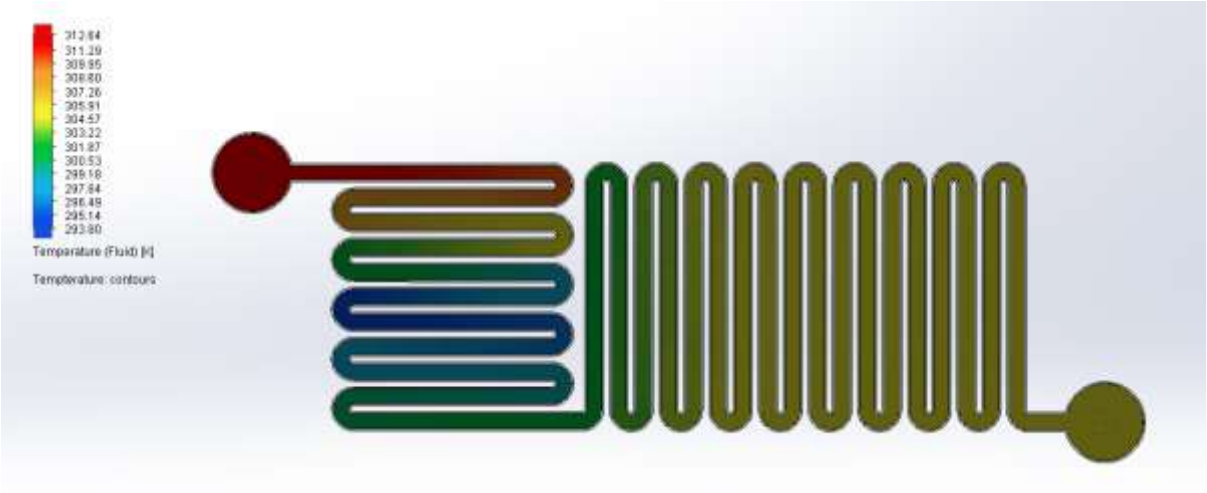

Fig. 6. Temperature contour within the microfluidic channel

3.5 Flow Trajectory

Figure 7 illustrates the flow trajectory and temperature contours of a 0.001 wt.% Al_2O_3-water nanofluid within a serpentine microfluidic channel. The flow trajectories, indicated by the directional arrows, highlight the fluid movement and interaction with the channel walls, while the color-coded temperature contours provide insight into the thermal distribution throughout the channel. The smooth, continuous lines suggest a laminar flow regime, which is typical in microfluidic systems due to the low Reynolds numbers [38]. The arrows' direction provides valuable information on fluid dynamics, including regions of high and low velocity, recirculation zones, and areas of potential flow separation. The red and orange arrows near the inlet indicate regions of higher velocity. These high-velocity zones are critical for ensuring that the fluid enters the microchannel with sufficient momentum to overcome resistance and maintain a steady flow. The presence of high velocities at the inlet also helps in achieving effective mixing and thermal management as the fluid progresses through the channel [39]. As the fluid navigates the serpentine path, the trajectories show areas of recirculation and mixing, particularly in the bends of the channel. These regions are marked by more densely packed arrows that change direction frequently. The recirculation zones enhance mixing and heat transfer by increasing the interaction between the fluid and the channel walls [40]. This improved interaction is essential for applications that require uniform temperature distribution and efficient heat dissipation. The color-coded temperature contours, ranging from red (highest temperature) to blue (lowest temperature), provide additional context to the flow trajectories. Near the inlet, the fluid is at its highest temperature (around 311.24 K), gradually cooling down as it moves through the channel. The combination of flow trajectories and temperature contours indicates that the fluid loses heat progressively, with the temperature dropping as the fluid moves through the serpentine path. The green and blue arrows in the mid and outlet sections of the channel indicate lower velocity regions. These areas are crucial for understanding the flow dynamics, as low velocities can lead to longer residence times, enhancing heat transfer and mixing. The presence of low-velocity

zones also suggests that the fluid has more time to interact with the channel walls, improving the overall thermal performance of the microfluidic system. The flow trajectory analysis highlights the effectiveness of the serpentine microfluidic channel in managing fluid dynamics and thermal distribution [41]. The laminar flow regime, combined with strategic recirculation zones, ensures efficient mixing and heat transfer. The temperature contours indicate that the nanofluid maintains a steady thermal gradient, which is crucial for applications requiring precise temperature control, such as biochemical assays, electronic cooling, and chemical reactions.

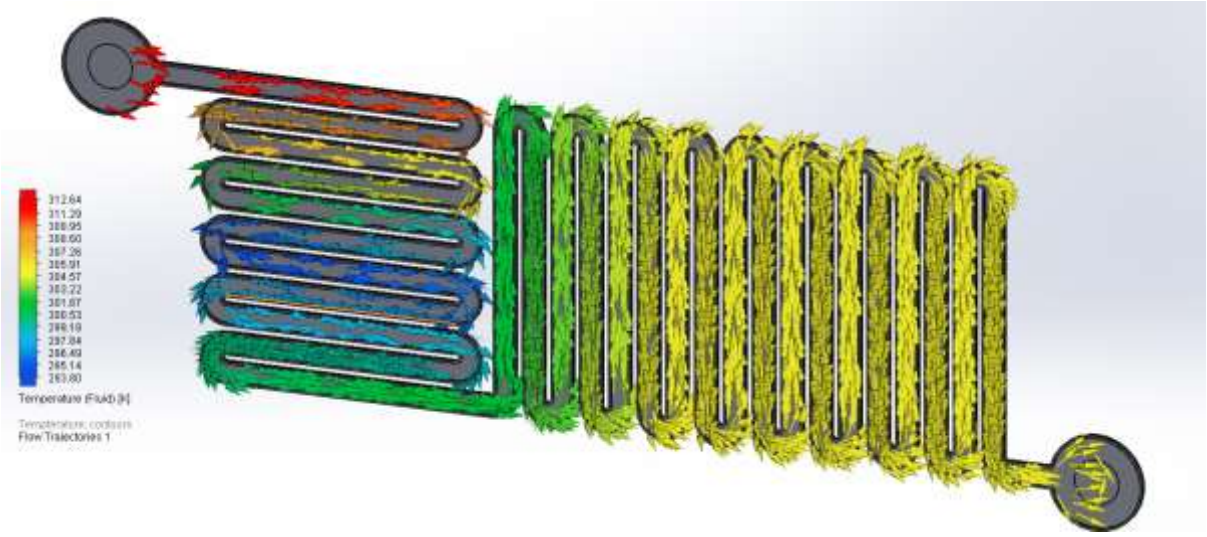

Fig. 7. Flow trajectory and temperature contours

By ensuring that key parameters in the simulations correspond directly to those in the experiments, an equivalent relationship between the two has been established. The consistency in results for pressure drop, temperature distribution, and velocity profiles indicates that the simulation model accurately reflects the experimental behavior. This equivalence suggests that the simulation can be used as a reliable tool for predicting the performance of nanofluids in microfluidic systems under similar conditions.

4. Conclusions

This study investigated the thermal and flow characteristics of a low-concentration alumina (Al_2O_3) nanofluid within a microfluidic system. Results demonstrated that even at a 0.001 wt.% concentration, alumina nanofluids can enhance thermal conductivity by up to 0.30%, without significantly affecting viscosity or flow behavior. The laminar flow regime was maintained, with a consistent pressure gradient and effective heat dissipation across the serpentine microchannel. The simulations aligned closely with experimental data, confirming the validity of the model. Overall, the study shows that low-concentration nanofluids have the potential for thermal management applications in microfluidic systems, with minimal impact on fluid dynamics. Future work should explore higher nanoparticle concentrations and long-term stability to further optimize system performance. The slight increase in thermal conductivity and the stable flow behavior makes Al_2O_3 nanofluids suitable for applications requiring precise temperature control and efficient heat dissipation, such as electronic cooling and chemical reactions. Future research should explore higher nanoparticle concentrations and different base fluids to further optimize the thermal and flow properties of nanofluids in microfluidic systems. Additionally, investigating the long-term stability and potential aggregation of nanoparticles in these systems will be crucial for practical applications.

Acknowledgment

The authors would like to thank the Universiti Malaysia Pahang Al-Sultan Abdullah for providing a research grant under no. UIC230821 and RDU232409.

References

[1] Ferreira, Mariana, Violeta Carvalho, João Ribeiro, Rui A. Lima, Senhorinha Teixeira, and Diana Pinho. "Advances in microfluidic systems and numerical modeling in biomedical applications: a review." *Micromachines* 15, no. 7 (2024): 873. https://doi.org/10.3390/mi15070873

[2] Lei, Xuehui, Weiwu Ye, F. Safdarin, and Sh Baghaei. "Microfluidics devices for sports: A review on technology for biomedical application used in fields such as biomedicine, drug encapsulation, preparation of nanoparticles, cell targeting, analysis, diagnosis, and cell culture." *Tissue and Cell* 87 (2024): 102339. https://doi.org/10.1016/j.tice.2024.102339

[3] Wong, Whui Dhong, Mohd Fadhil Majnis, Chin Wei Lai, Suresh Sagadevan, and Nurhidayatullaili Muhd Julkapli. "Enhancement of mixing and reaction efficiency of various fluids applications at different microfluidic configuration and design." *Chemical Engineering and Processing-Process Intensification* (2024): 109729. https://doi.org/10.1016/j.cep.2024.109729

[4] Samylingam, Lingenthiran, Navid Aslfattahi, Chee Kuang Kok, Kumaran Kadirgama, Norazlianie Sazali, Michal Schmirler, Devarajan Ramasamy, Wan Sharuzi Wan Harun, Mahendran Samykano, and A. S. Veerendra. "Green Engineering with Nanofluids: Elevating Energy Efficiency and Sustainability." *Journal of Advanced Research in Micro and Nano Engineering* 16, no. 1 (2024): 19-34. https://doi.org/10.37934/armne.16.1.1934

[5] Samylingam, Lingenthiran, Navid Aslfattahi, Chee Kuang Kok, Kumaran Kadirgama, Norazlianie Sazali, Kia Wai Liew, Michal Schmirler et al., "Enhancing Lubrication Efficiency and Wear Resistance in Mechanical Systems through the Application of Nanofluids: A Comprehensive Review." *Journal of Advanced Research in Micro and Nano Engineering* 16, no. 1 (2024): 1-18. https://doi.org/10.37934/armne.16.1.118

[6] Muthusamy, Y., K. Kadirgama, M. M. Rahman, D. Ramasamy, and K. V. Sharma. "Wear analysis when machining AISI 304 with ethylene glycol/TiO 2 nanoparticle-based coolant." *The International Journal of Advanced Manufacturing Technology* 82 (2016): 327-340. https://doi.org/10.1007/s00170-015-7360-3

[7] Souza, Reinaldo R., Inês M. Gonçalves, Raquel O. Rodrigues, Graca Minas, J. M. Miranda, Antonio LN Moreira, Rui Lima, Goncalo Coutinho, J. E. Pereira, and Ana S. Moita. "Recent advances on the thermal properties and applications of nanofluids: From nanomedicine to renewable energies." *Applied Thermal Engineering* 201 (2022): 117725. https://doi.org/10.1016/j.applthermaleng.2021.117725

[8] Ohenhen, Peter Efosa, Onyinyechukwu Chidolue, Aniekan Akpan Umoh, Bright Ngozichukwu, Adetomilola Victoria Fafure, Valentine Ikenna Ilojianya, and Kenneth Ifeanyi Ibekwe. "Sustainable cooling solutions for electronics: A comprehensive review: Investigating the latest techniques and materials, their effectiveness in mechanical applications, and associated environmental benefits." *World Journal of Advanced Research and Reviews* 21, no. 1 (2024): 957-972.

[9] Kumar, Raj, Daeho Lee, Ümit Ağbulut, Sushil Kumar, Sashank Thapa, Abhishek Thakur, R. D. Jilte, C. Ahamed Saleel, and Saboor Shaik. "Different energy storage techniques: recent advancements, applications, limitations, and efficient utilization of sustainable energy." *Journal of Thermal Analysis and Calorimetry* 149, no. 5 (2024): 1895-1933. https://doi.org/10.1007/s10973-023-12831-9

[10] Narvaez, Javier A., Hugh Thornburg, Markus P. Rumpfkeil, and Robert J. Wilkens. "Computational modeling of a microchannel cold plate: Pressure, velocity, and temperature profiles." *International Journal of Heat and Mass Transfer* 78 (2014): 90-98. https://doi.org/10.1016/j.ijheatmasstransfer.2014.06.006

[11] Roy, Abin, K. P. Venkitaraj, Pethurajan Vigneshwaran, Shaik Saboor, Erdem Cuce, and Kuldeep K. Saxena. "Enhanced convective heat transfer with Al2O3-water nanofluid in a PCM-based thermal energy storage system." *Journal of Energy Storage* 97 (2024): 112853. https://doi.org/10.1016/j.est.2024.112853

[12] Hussein, A. M., Lingenthiran, K. Kadirgamma, M. M. Noor, and L. K. Aik. "Palm oil based nanofluids for enhancing heat transfer and rheological properties." *Heat and Mass Transfer* 54 (2018): 3163-3169. https://doi.org/10.1007/s00231-018-2364-9

[13] Samylingam, I., K. Kadirgama, Navid Aslfattahi, L. Samylingam, D. Ramasamy, W. S. W. Harun, M. Samykano, and R. Saidur. "Review on thermal energy storage and eutectic nitrate salt melting point." In *IOP Conference Series: Materials Science and Engineering*, vol. 1078, no. 1, p. 012034. IOP Publishing, 2021. https://doi.org/10.1088/1757-899X/1078/1/012034

[14] Koo, Junemoo, and Clement Kleinstreuer. "Laminar nanofluid flow in microheat-sinks." *International journal of heat and mass transfer* 48, no. 13 (2005): 2652-2661. https://doi.org/10.1016/j.ijheatmasstransfer.2005.01.029

[15] Puliti, Gianluca. "Properties of Gold-Water Nanofluids Using Molecular Dynamics." PhD diss., University of Notre Dame, 2012.
[16] Soares, Yago Chamoun F., Dante Daiki Yokoyama, Lidiane Cristina Costa, Josué Marciano de Oliveira Cremonezzi, Hélio Ribeiro, Mônica Feijó Naccache, and Ricardo Jorge E. Andrade. "Multifunctional hexagonal boron nitride dispersions based in xanthan gum for use in drilling fluids." *Geoenergy Science and Engineering* 221 (2023): 111311. https://doi.org/10.1016/j.petrol.2022.111311
[17] Shahrul, I. M., I. M. Mahbubul, S. S. Khaleduzzaman, R. Saidur, and M. F. M. Sabri. "A comparative review on the specific heat of nanofluids for energy perspective." *Renewable and sustainable energy reviews* 38 (2014): 88-98. https://doi.org/10.1016/j.rser.2014.05.081
[18] Ramachandran, Kaaliarasan, Devarajan Ramasamy, Mahendran Samykano, Lingenthiran Samylingam, Faris Tarlochan, and Gholamhassan Najafi. "Evaluation of specific heat capacity and density for cellulose nanocrystal-based nanofluid." *Journal of Advanced Research in Fluid Mechanics and Thermal Sciences* 51, no. 2 (2018): 169-186.
[19] Vega-Sánchez, Christopher, and Chiara Neto. "Pressure drop measurements in microfluidic devices: a review on the accurate quantification of interfacial slip." *Advanced Materials Interfaces* 9, no. 5 (2022): 2101641. https://doi.org/10.1002/admi.202101641
[20] Gorbunov, Dmitry, Maria Nenasheva, Gregory Shashkin, Viktor Shapovalov, Petr Shvets, Evgeny Naranov, Anton Maximov, Alexander Guda, and Alexander Soldatov. "Transferring hydroformylation reaction into high-pressure gas-liquid microfluidic systems: key achievements and perspectives." *Journal of Industrial and Engineering Chemistry* (2024). https://doi.org/10.1016/j.jiec.2024.02.029
[21] Azizov, Ilgar, Marcin Dudek, and Gisle Øye. "Studying droplet retention in porous media by novel microfluidic methods." *Chemical Engineering Science* 248 (2022): 117152. https://doi.org/10.1016/j.ces.2021.117152
[22] Naseri, Mahdi, George P. Simon, and Warren Batchelor. "Development of a paper-based microfluidic system for a continuous high-flow-rate fluid manipulation." *Analytical Chemistry* 92, no. 10 (2020): 7307-7316. https://doi.org/10.1021/acs.analchem.0c01003
[23] Sun, Jindi. *Quantitative Analysis of Flow Through Permeable Media in Microfluidic Devices*. University of Wyoming, 2022.
[24] Xiong, Tong, Guoqiang Liu, Shenjie Huang, Gang Yan, and Jianlin Yu. "Two-phase flow distribution in parallel flow mini/micro-channel heat exchangers for refrigeration and heat pump systems: A comprehensive review." *Applied Thermal Engineering* 201 (2022): 117820. https://doi.org/10.1016/j.applthermaleng.2021.117820
[25] Leschziner, Michael A. "Friction-drag reduction by transverse wall motion–a review." *Journal of Mechanics* 36, no. 5 (2020): 649-663. https://doi.org/10.1017/jmech.2020.31
[26] Lee, Jing Jei. *Studying Droplet Behavior and Capillary flow in Open Microfluidic Channels*. University of Washington, 2021.
[27] Ulkir, Osman, Oguz Girit, and Ishak Ertugrul. "Design and Analysis of a Laminar Diffusion-Based Micromixer with Microfluidic Chip." *Journal of Nanomaterials* 2021, no. 1 (2021): 6684068. https://doi.org/10.1155/2021/6684068
[28] Liu, Suhong, Dariush Bahrami, Rasool Kalbasi, Mehdi Jahangiri, Ye Lu, Xuelan Yang, Shahab S. Band, Kwok-Wing Chau, and Amir Mosavi. "Efficacy of applying discontinuous boundary condition on the heat transfer and entropy generation through a slip microchannel equipped with nanofluid." *Engineering Applications of Computational Fluid Mechanics* 16, no. 1 (2022): 952-964. https://doi.org/10.1080/19942060.2022.2057591
[29] Foroushani, Sepehr, David Naylor, and John L. Wright. "Heat transfer correlations for laminar free convection in vertical channels with asymmetrically heated isothermal walls." *Heat Transfer Engineering* (2020). https://doi.org/10.1080/01457632.2018.1558015
[30] Zhang, Xuelai, Zhe Ji, Jifen Wang, and Xin Lv. "Research progress on structural optimization design of microchannel heat sinks applied to electronic devices." *Applied Thermal Engineering* (2023): 121294. https://doi.org/10.1016/j.applthermaleng.2023.121294
[31] Cramer, Corson L., Emanuel Ionescu, Magdalena Graczyk-Zajac, Andrew T. Nelson, Yutai Katoh, Jeffery J. Haslam, Lothar Wondraczek et al., "Additive manufacturing of ceramic materials for energy applications: Road map and opportunities." *Journal of the European Ceramic Society* 42, no. 7 (2022): 3049-3088. https://doi.org/10.1016/j.jeurceramsoc.2022.01.058
[32] Dos-Reis-Delgado, Alejandro A., Andrea Carmona-Dominguez, Gerardo Sosa-Avalos, Ivan H. Jimenez-Saaib, Karen E. Villegas-Cantu, Roberto C. Gallo-Villanueva, and Víctor H. Perez-Gonzalez. "Recent advances and challenges in temperature monitoring and control in microfluidic devices." *Electrophoresis* 44, no. 1-2 (2023): 268-297. https://doi.org/10.1002/elps.202200162
[33] Khater, Asmaa, Osama Abdelrehim, Mehdi Mohammadi, Abdulmajeed Mohamad, and Amir Sanati-Nezhad. "Thermal droplet microfluidics: From biology to cooling technology." *TrAC Trends in Analytical Chemistry* 138 (2021): 116234. https://doi.org/10.1016/j.trac.2021.116234

[34] Sankad, G. C., G. Durga Priyadarsini, Magda Abd El-Rahman, M. R. Gorji, and Nizar Abdallah Alsufi. "Microfluidics temperature compensation and tracking for drug injection based on mechanically pulsating heat exchanger." *Journal of Thermal Analysis and Calorimetry* 148, no. 21 (2023): 12059-12070. https://doi.org/10.1007/s10973-023-12520-7

[35] Huang, Yicheng, Xuelian Xiao, Huifang Kang, Jianguo Lv, Rui Zeng, and Jun Shen. "Thermal management of polymer electrolyte membrane fuel cells: A critical review of heat transfer mechanisms, cooling approaches, and advanced cooling techniques analysis." *Energy Conversion and Management* 254 (2022): 115221. https://doi.org/10.1016/j.enconman.2022.115221

[36] Khaji, Zahra, and Maria Tenje. "Integrated cooling system for microfluidic PDMS devices used in biological microscopy studies." *Journal of Micromechanics and Microengineering* 32, no. 8 (2022): 087001. https://doi.org/10.1088/1361-6439/ac7772

[37] Kadirgama, K., L. Samylingam, Navid Aslfattahi, M. Samykano, D. Ramasamy, and R. Saidur. "Experimental investigation on the optical and stability of aqueous ethylene glycol/mxene as a promising nanofluid for solar energy harvesting." In *IOP Conference Series: Materials Science and Engineering*, vol. 1062, no. 1, p. 012022. IOP Publishing, 2021. https://doi.org/10.1088/1757-899X/1062/1/012022

[38] Yuan, Shuai, Bingyan Jiang, Tao Peng, Qiang Li, and Mingyong Zhou. "An investigation of flow patterns and mixing characteristics in a cross-shaped micromixer within the laminar regime." *Micromachines* 12, no. 4 (2021): 462. https://doi.org/10.3390/mi12040462

[39] Gao, Jie, Zhuohuan Hu, Qiguo Yang, Xing Liang, and Hongwei Wu. "Fluid flow and heat transfer in microchannel heat sinks: Modelling review and recent progress." *Thermal Science and Engineering Progress* 29 (2022): 101203. https://doi.org/10.1016/j.tsep.2022.101203

[40] Liu, Lin, Ziyong Cao, Chao Xu, Ling Zhang, and Te Sun. "Investigation of fluid flow and heat transfer characteristics in a microchannel heat sink with double-layered staggered cavities." *International Journal of Heat and Mass Transfer* 187 (2022): 122535. https://doi.org/10.1016/j.ijheatmasstransfer.2022.122535

[41] Arockiam, Siril, Yu Hsuan Cheng, Piero M. Armenante, and Sagnik Basuray. "Experimental determination and computational prediction of the mixing efficiency of a simple, continuous, serpentine-channel microdevice." *Chemical Engineering Research and Design* 167 (2021): 303-317. https://doi.org/10.1016/j.cherd.2021.01.022